Supporting informations for

Short Wave Infrared Devices Based on HgTe Nanocrystals with Air Stable Performances

Amardeep Jagtap[1], Nicolas Goubet[1,2], Clément Livache[1,2], Audrey Chu[1], Bertille Martinez[1,2], Charlie Gréboval[1], Junling Qu[1], Erwan Dandeu[1], Loïc Becerra[1], Nadine Witkowski[1], Sandrine Ithurria[2], Fabrice Mathevet[3], Mathieu G. Silly[4], Benoit Dubertret[2], Emmanuel Lhuillier[1*]

[1]Sorbonne Université, CNRS, Institut des NanoSciences de Paris, INSP, F-75005 Paris, France
[2]Laboratoire de Physique et d'Etude des Matériaux, ESPCI-Paris, PSL Research University, Sorbonne Université UPMC Univ Paris 06, CNRS, 10 rue Vauquelin 75005 Paris, France.
[3]Sorbonne Université, Institut Parisien de Chimie Moléculaire, UMR 8232, Chimie des Polymères, 4 Place Jussieu, 75252 Paris Cedex 05, France
[4]Synchrotron-SOLEIL, Saint-Aubin, BP48, F91192 Gif sur Yvette Cedex, France.

Table of contents

1. Material characterization

1.1. Photoemission measurements

Photoemission measurements have been conducted on the TEMPO beamline of synchrotron Soleil. Experimental details are given in the supporting information of ref. 1. Photoemission is used to determine the work function (4.7 eV, see Figure S 1a) and the position of the valence band with respect to the Fermi level (Figure S 1b).
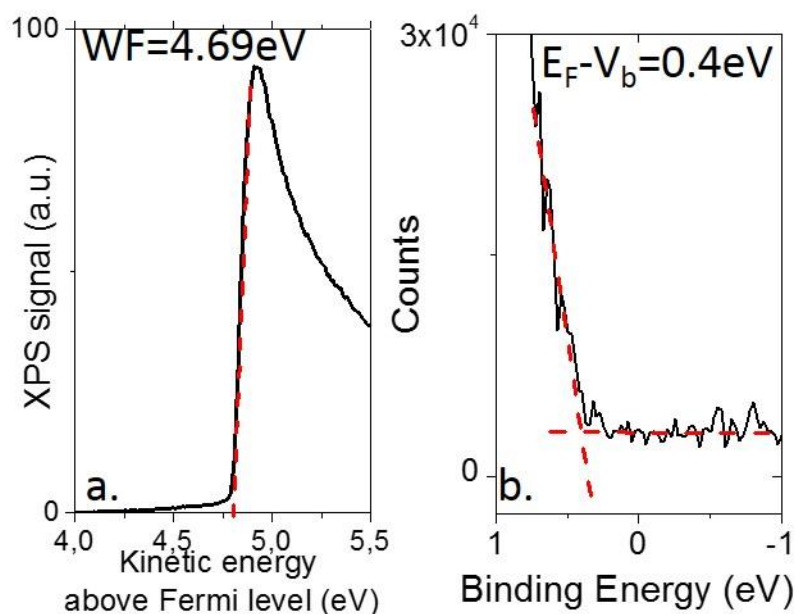

Figure S 1. X-ray photoemission spectrum of the valence band from HgTe CQDs around the cut off of the secondary electron (part a) and close to the Fermi level (part b). Adapted with permission from ref 1. Copyright (2018) American Chemical Society.

1.2. Transient photocurrent measurement to determine Urbach energy

We build a specific setup to obtain transient photocurrent measurement with a broad signal and temporal dynamics, see Figure S 2. To conduct this measurement, a pulsed laser (Crylas FTSS 355-50) at 355 nm is used. To prevent excessive heating of the sample which may lead to a drift of the photoresponse, the laser beam is around 1 mm in diameter (*i.e.*, poorly focused). The pulses are 1 ns long and repeated every 10 ms (100 Hz). A photodiode is used to trigger the signal. The sample is placed in a vacuum chamber. The bias, 30 V is applied by a Keithley 2432b. The bias is higher than the applied electric field for transistor measurement in order to boost the signal. An oscilloscope (Rohde & Schwarz, RTE 1102) acquires the outcoming signal through a 50 Ω resistor, hence analyzing a voltage proportional to I_{DS}. On the second part of the signal, we observe that conductance follows a power law as a function

of time. The power exponent (α) is directly related to the Urbach tail energy (Eu) using the formula: $\alpha = \dfrac{k_b T}{E_u} - 1$
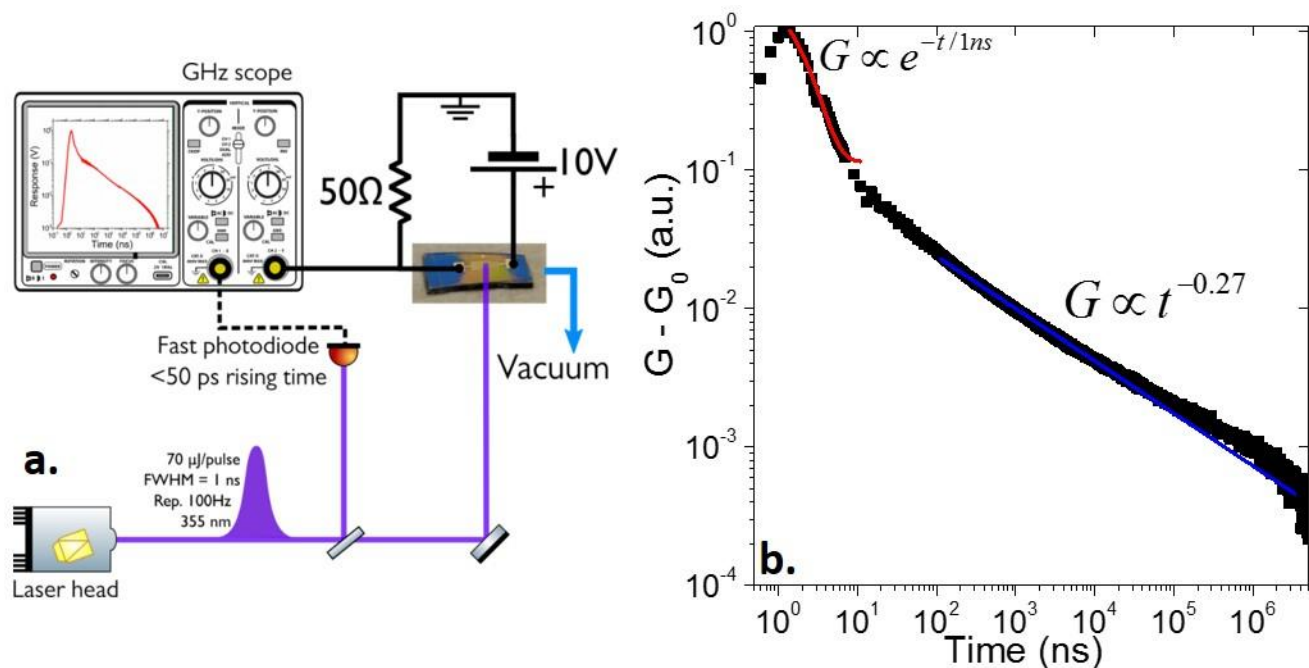

Figure S 2 - a. Scheme of the transient photocurrent setup. b. Transient photocurrent of a HgTe CQD film capped with EDT ligands in response to a 1 ns pulse of light at 355 nm. Adapted with permission from ref 1. Copyright (2018) American Chemical Society.

1.3. Effect of annealing on the physical propertries of HgTe CQD films

The effect of annealing on HgTe CQD film is discussed in Figure S 3. Annealing above 50 °C leads to a broadening of the excitonic peak (Figure S 3a) and to a rise of the film conductance (Figure S 3b and c)
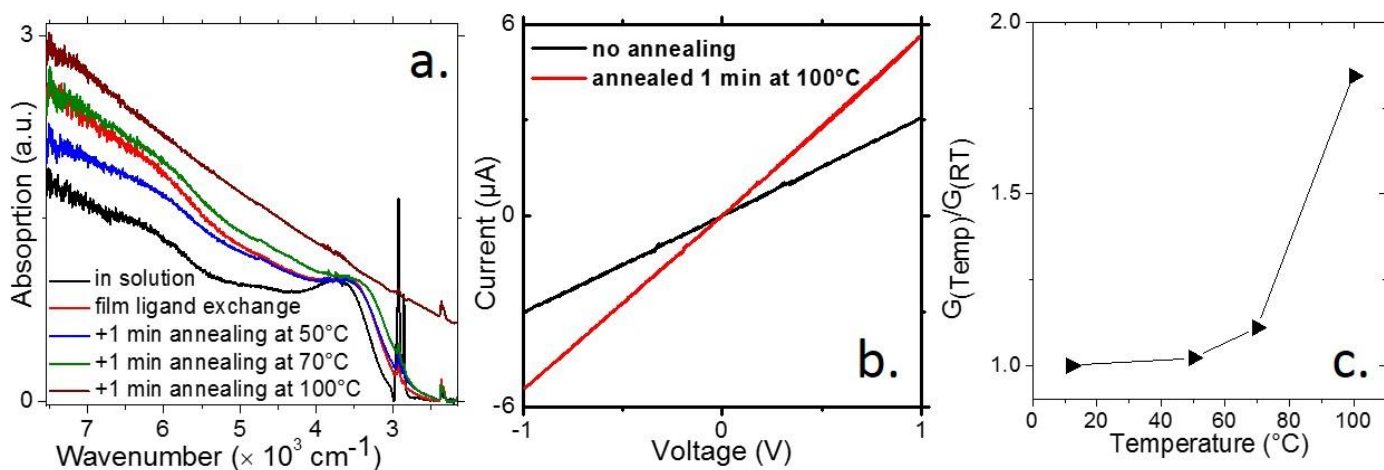

Figure S 3 - a. Infrared spectrum of a HgTe CQD film in solution and on film after ligand exchange and after annealing at different temperatures for 1 min. c Dark I-V curve for a HgTe CQD film capped with EDT, for a non-annealed film and for a film annealed 1 min at 100 °C. c. Ratio of conductance for a HgTe CQD film capped with EDT as a function of the annealing temperature, conducted for 1 min. RT stands for room temperature.

2. Device fabrication and structure

2.1. Effect of encapuslation layers on the temperature dependence of HgTe CQD films

The temperature dependence of the film in photoconductive mode, without and with protective layers, are given respectively, on Figure S 4a. and b. Without the protective layer the device presents non-monotonic temperature dependence (*i.e.* in other words, cooling is useless), this issue was fixed by the addition of the protective layers. In photoconductive mode and with protective layers, the current follows an Arrhenius law around room temperature with 114 meV activation energy. Once the HgTe layer was integrated into the photovoltaic device with encapsulation layers, a similar behavior and magnitude of the activation energy (120 meV) is measured, see Figure S 4c.
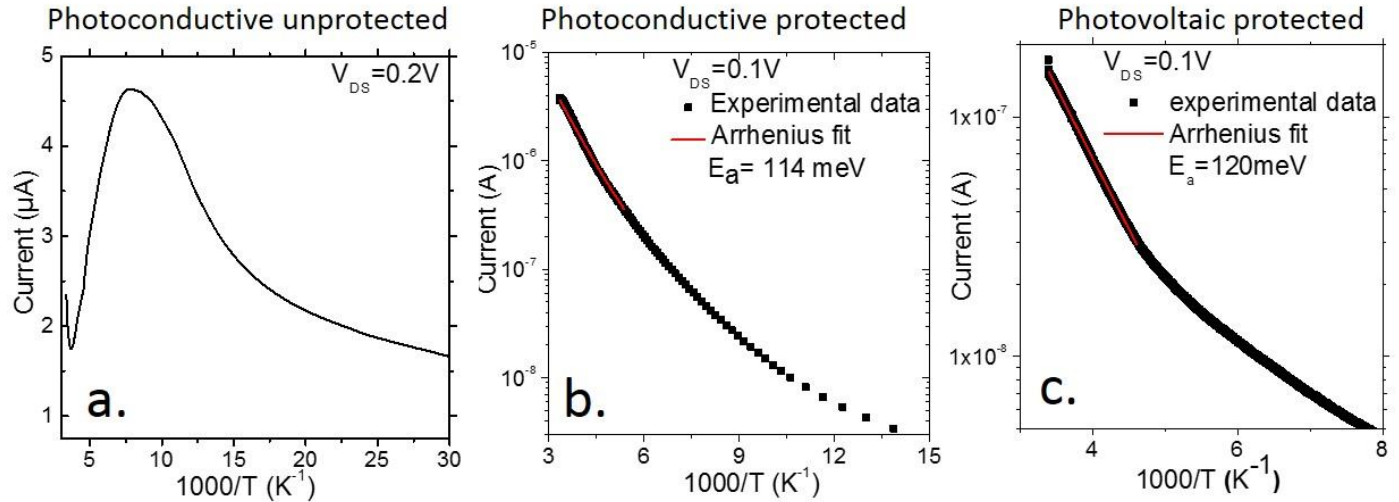

Figure S 4 - a. Current as a function of temperature for a HgTe CQD film (photoconductive configuration) capped with EDT without protective layer. b. Current as a function of temperature for a HgTe CQD film (photoconductive configuration) capped with EDT with the protective layers. c. Current as a function of temperature for a HgTe CQD film (photovoltaic configuration) capped with EDT with the protective layers

2.2. Transmission of glass ITO substrate- and protective layers

To design PV device in the SWIR, we use conventional glass/ITO layer, see Figure S 5a. However compared to solar cell, we choose to use thinner ITO layer (30 nm typically), to reduce the absorption of the transparent electrodes. We also have checked the transmission of the protective encapsulation layer, which is also quite transparent in the near and even mid IR range, see Figure S 5b.
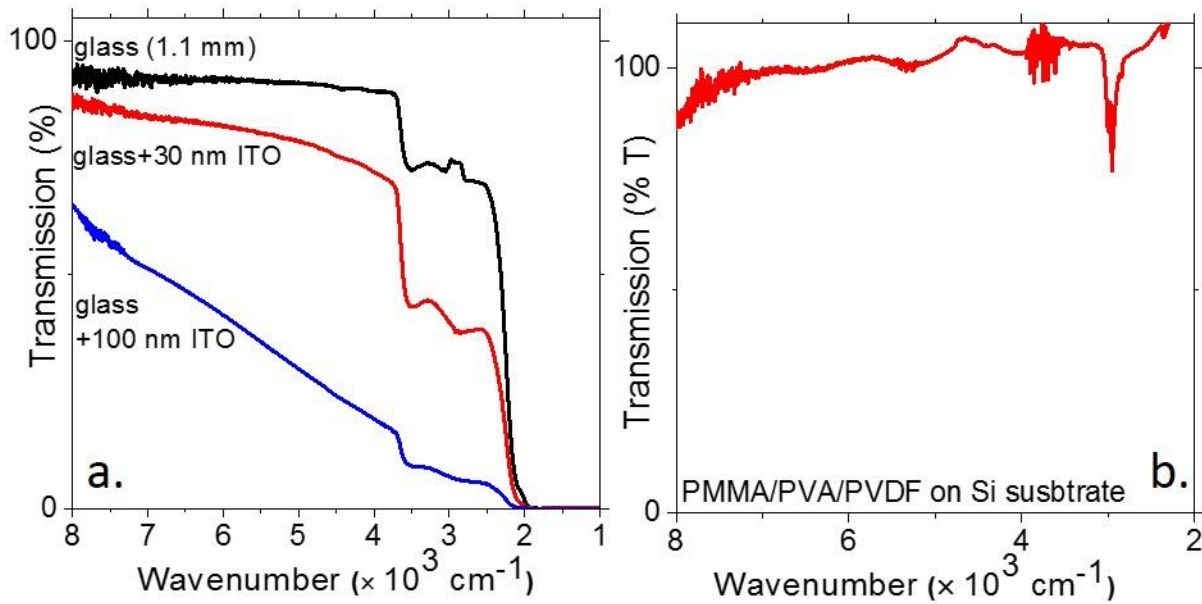
Figure S 5. a. Infrared spectra of 1.1 mm thick glass slide coated with various thickness of ITO as mentioned in the graph. b. Transmission spectrum of PMMA/PVA/PVDF layer in the infrared

2.3. Band alignment for PV device

We estimate the band alignment of our diode to be given by Figure S 6. HgTe has a narrower band gap compared to PbS CQDs, which are used for solar cell. As a result, some photoelectrons get filtered by the TiO_2 layer.

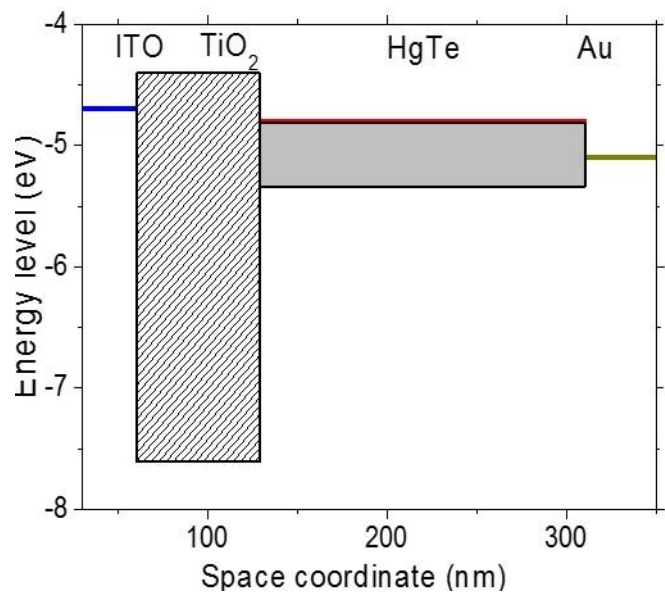*Figure S 6 Band alignment of the ITO/TiO₂/HgTe/Au photovoltaic structure.*

3. Device Performances

3.1. Noise measurements

A scheme of the setup used for the noise measurement is given in Figure S 7. Basically, the sample is biased using the input of a DLPCA 200 amplifier. The signal is then amplified and acquired on a SR780 spectrum analyzer.
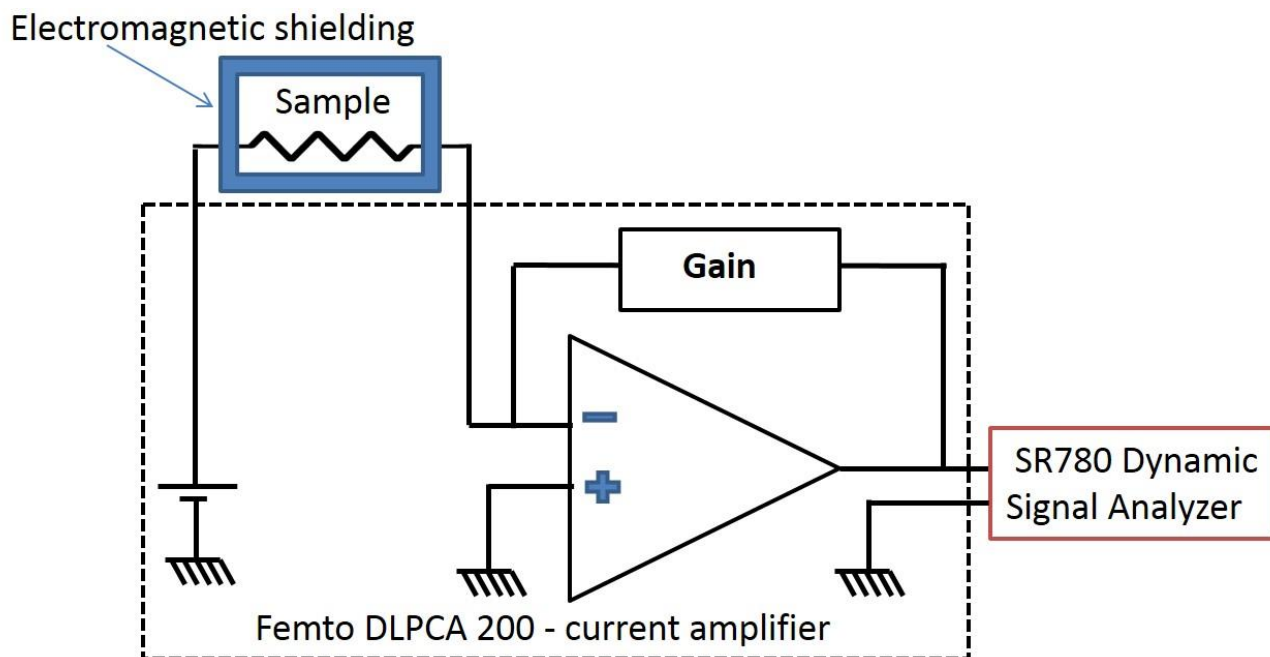

Figure S 7. Scheme of the setup for the noise measurement

3.2. Setup for frequency response

Calibrated blackbody source (Omega, BB4) is set to 1200 K and a high pass Germanium filter is used to cut down electromagnetic radiation below 1.8 μm. The device is aligned with blackbody cavity such as the angle between the detector normal and the light path is 0°. A lock-in amplifier (model MFLI from Zurich instrument) is used to obtain the IR photo-generated signal from the device using mechanical chopper. See Figure S 8 for a scheme of the setup.
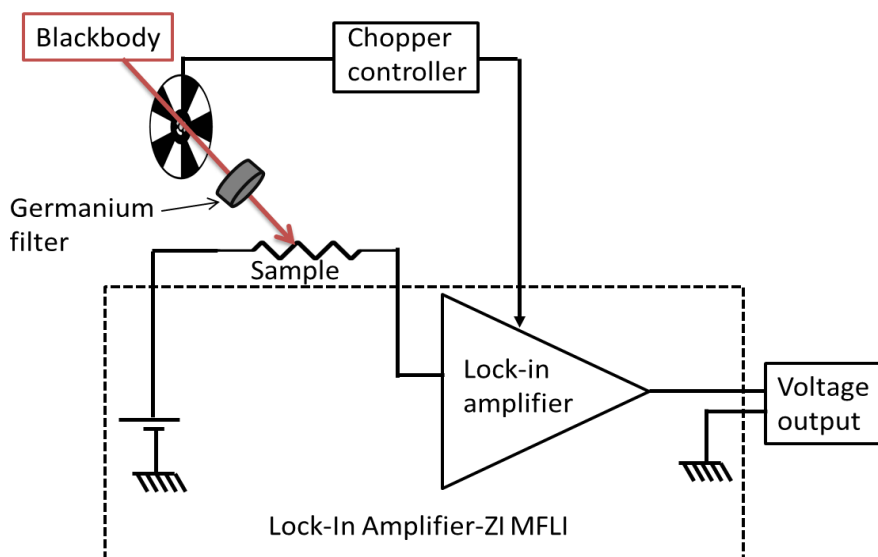
For frequency dependent photocurrent measurements with 1.5 µm laser diode, the samples are biased using Keithley 2634b and modulation up to 10 kHz is achieved using electrical chopping. Thus, obtained photo-generated signal from sample is first amplified using DLPCA-200 current amplifier and subsequently fed to oscilloscope.

3.3. Performances of photoconductive device

Figure S 9 presents the device characterization relative to the photoconductive device. Figure S 9a and b discuss the time response of the device and demonstrate a bandwidth above 10 kHz. Figure S 9c and d show the noise current density in the device and clearly show a prevailing 1/f contribution for the noise. Figure S 9e shows the responsivity of the device under blackbody illumination. Responsivity is in the 1 to 10 mA.W^{-1} range depending on the applied bias.
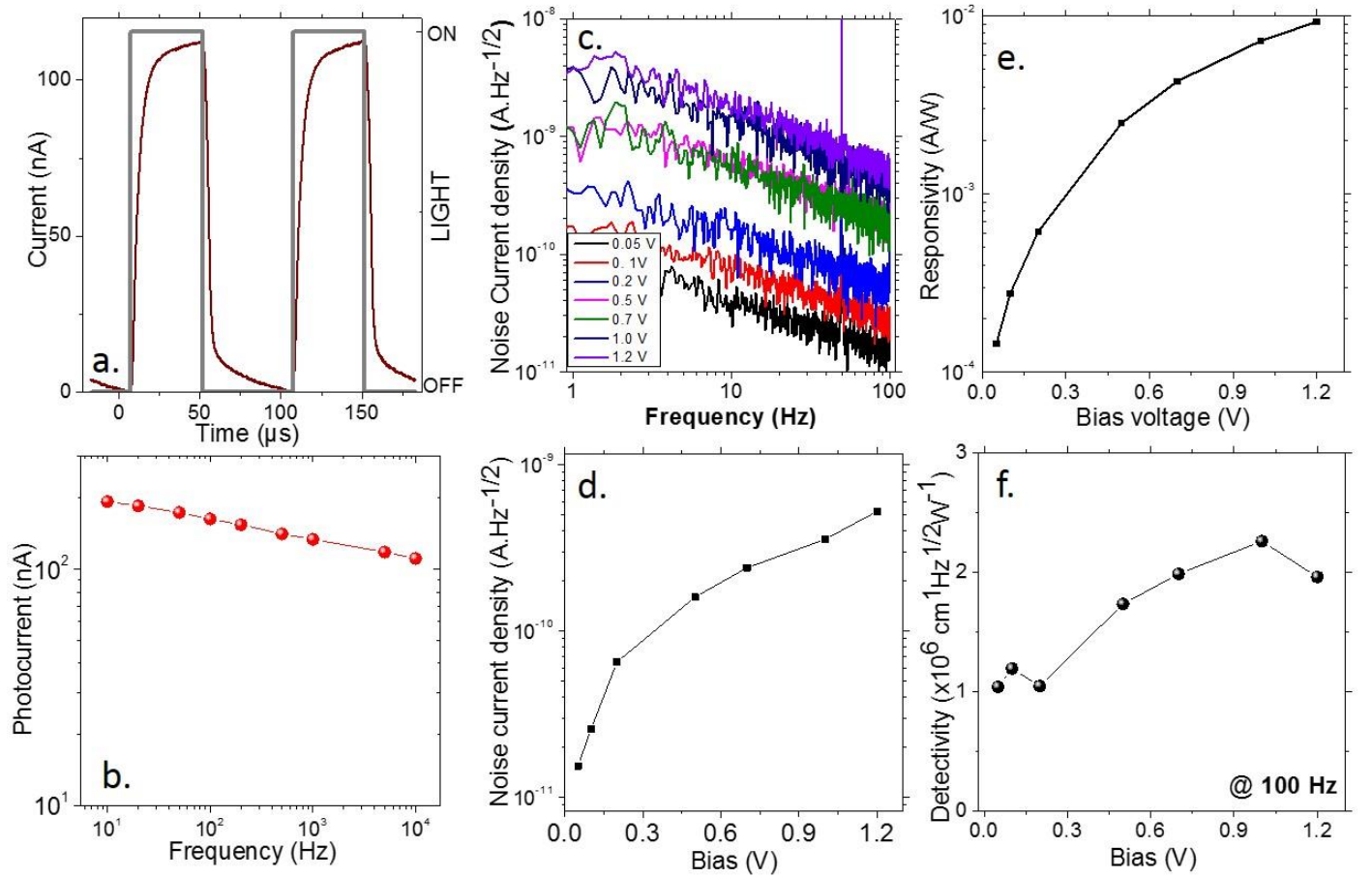

Figure S 9 - Performances of protected planar photodetector a. Photocurrent as a function of time for a HgTe CQD film in a photoconductive configuration, while the light (λ=1.55 µm) is turned on and off with a frequency of 10 kHz. b. Bode diagram of the photocurrent intensity for a HgTe CQD film in a photoconductive configuration, as a function of the light chopping frequency. c. Noise current density as a function of frequency for a HgTe CQD film in a photoconductive configuration under different biases. d. Noise current density (at 100 Hz) as a function of applied bias for a HgTe CQD film in a photoconductive configuration. e Responsivity as a function of the applied bias under blackbody illumination (T$_{BB}$= 927 °C) for a HgTe CQD film in a photoconductive configuration. f. Room temperature detectivity at 100 Hz, as a function of the applied bias for a HgTe CQD film in a photoconductive configuration.

3.4. Performances of photovoltaic device

Figure S 10 presents the device characterization relative to the photodiode device. Figure S 10a and b discuss the time response of the device and also demonstrate a bandwidth above 10 kHz. Figure S 10c and d show the noise magnitude. As for photoconductive mode, *1/f* contribution is still the prevailing contribution. We can note a clear decrease of the noise magnitude compared to photoconductive mode, in the low bias range. Figure S 10e shows the responsivity of the device under blackbody (at 1200 °K) illumination. Responsivity is typically reduced by an order of magnitude compared to photoconductive mode, which suggests a limited efficiency of the charge extraction, which is further confirmed when evaluation the internal quantum efficiency, which currently remains weak (0.3% and less), see Figure S 11. In the low bias range the reduction of the noise is nevertheless stronger than the loss of responsivity, which leads to detectivity as high as 10^7 jones, which is one decade above the value achieved in the photoconductive mode.
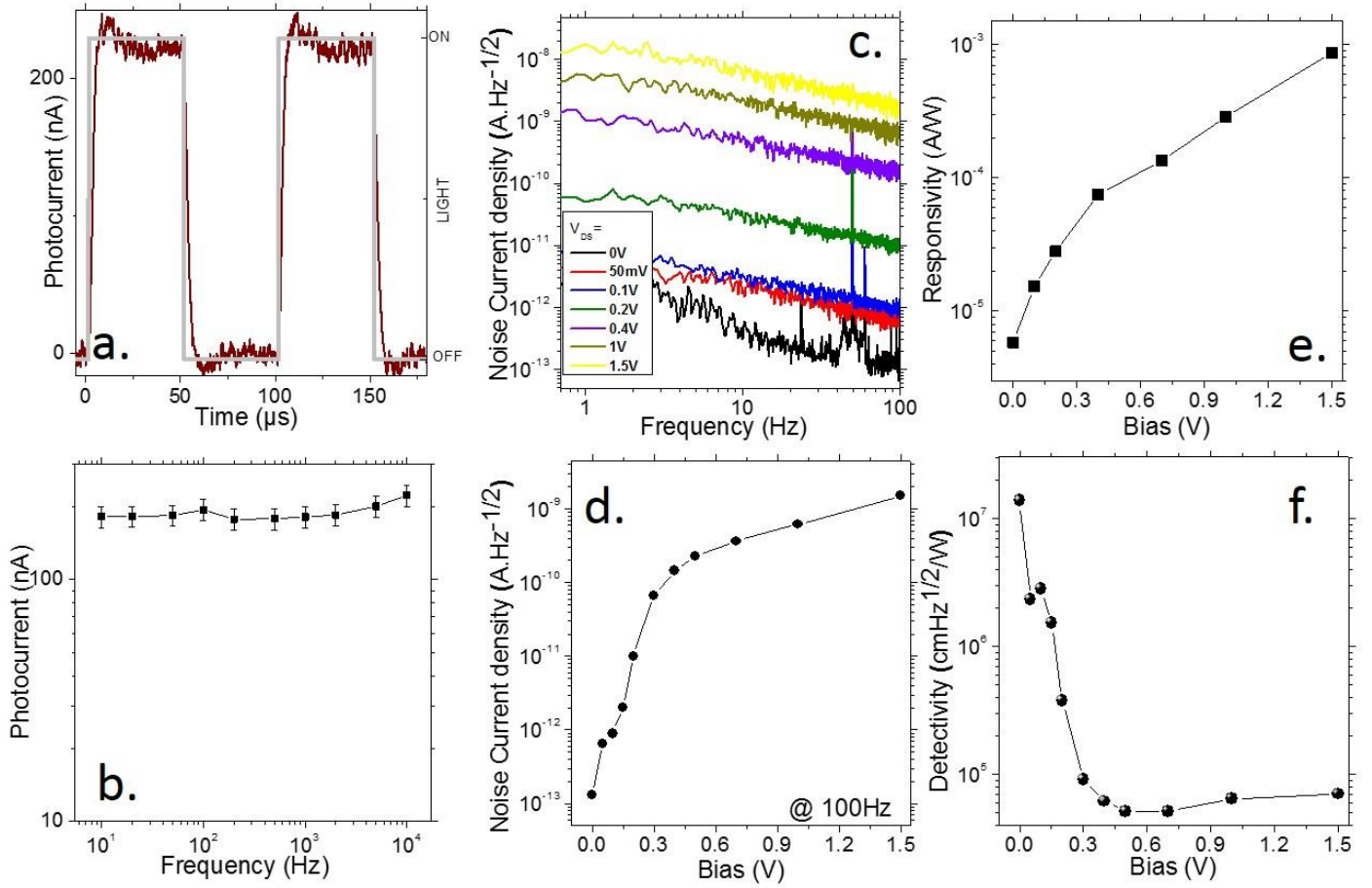

Figure S 10 - a. Current as a function of time for a HgTe CQD film in a photovoltaic configuration, while the light (λ=1.55 μm) is turned on and off with a frequency of 10 kHz. b. Bode diagram of the photocurrent intensity for a HgTe CQD film in a photoconductive configuration, as a function of the light chopping frequency. c. Noise current density (at 100 Hz) as a function of frequency for a HgTe CQD film in a photovoltaic configuration under different biases. d. Noise current density as a function of applied bias for a HgTe CQD film in a photovoltaic configuration. e. Responsivity as a function of the applied bias under blackbody illumination (T_{BB}= 927 °C) for a HgTe CQD film in a photovoltaic configuration. f. Room temperature detectivity at 100 Hz, as a function of the applied bias for a HgTe CQD film in a photovoltaic configuration.

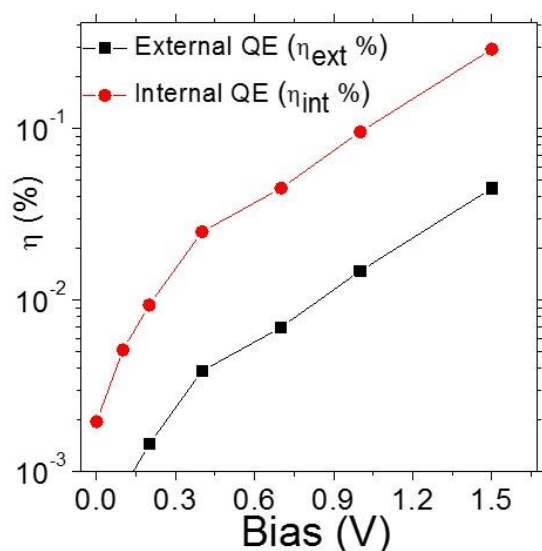## 3.5. Evaluation of the quantum efficiency for the PV device

Figure S 11 external and internal quantum efficiency for the photodiode as a function of the applied bias

3.6. Stability of the PV device

We have checked the stability of the PV device over a period of seven weeks, see Figure S 12. We notice very limited change in the dark and photocurrent.
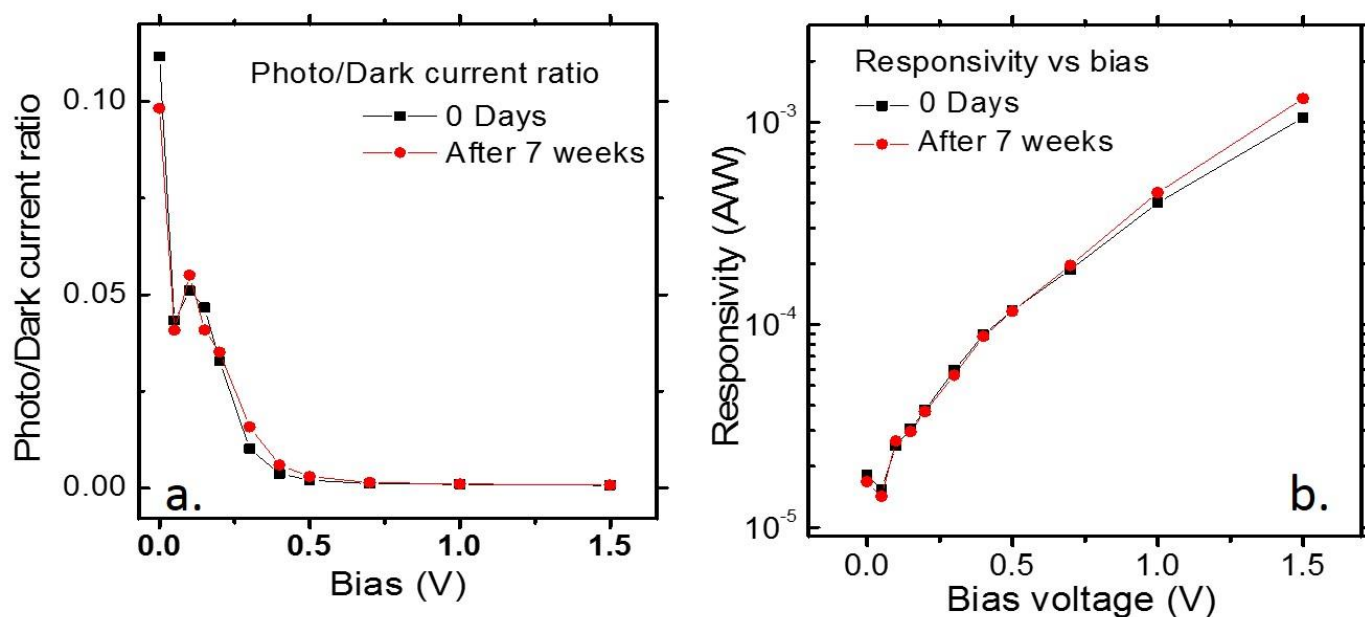

Figure S 12 a. photocurrent over dark current as a function of bias for a PV device at time zero and 7 weeks after its fabrication. b Responsivity as a function of bias for a PV device at time zero and 7 weeks after its fabrication

4. REFERENCES

[1] Martinez, B.; Livache, C.; Goubet, N.; Jagtap, A.; Cruguel, H.; Lacaze, E.; Silly, M. G.; Lhuillier, E. Probing Charge Carrier Dynamics to Unveil the Role of Surface Ligands on HgTe Narrow Band Gap Nanocrystals. *J. Phys. Chem. C* **2018**, *122*, 859–865.